JBMR Plus, 2024, **8**, ziae026
https://doi.org/10.1093/jbmrpl/ziae026
Advance access publication: March 4, 2024
Research Article

A homozygous *SP7/OSX* mutation causes osteogenesis and dentinogenesis imperfecta with craniofacial anomalies

Dalal A. Al-Mutairi[1,*], Ali A. Jarragh[2], Basel H. Alsabah[3], Marc N. Wein[4], Wasif Mohammed[5], Lateefa Alkharafi[6]

[1]Department of Pathology, Faculty of Medicine, Kuwait University, 13110 Kuwait City, Kuwait
[2]Department of Surgery, Faculty of Medicine, Kuwait University, 13110 Kuwait City, Kuwait
[3]Zain Specialized Hospital for Ear, Nose and Throat, 70030 Kuwait City, Kuwait
[4]Endocrine Unit, Massachusetts General Hospital, Harvard Medical School, Boston, MA 02114, United States
[5]Department of Radiology, Al Sabah Hospital, 13041 Kuwait City, Kuwait
[6]Cleft and Craniofacial Unit, Farwaniya Specialized Dental Center, Ministry of Health, 13001 Kuwait City, Kuwait
*Corresponding author: Dalal A. Al-Mutairi, Department of Pathology, Faculty of Medicine, Kuwait University, 13110 Kuwait City, Kuwait (Dalal.almutairi@ku.edu.kw)

Abstract

Osteogenesis imperfecta (OI) is a heterogeneous spectrum of hereditary genetic disorders that cause bone fragility, through various quantitative and qualitative defects of type 1 collagen, a triple helix composed of two α1 and one α2 chains encoded by *COL1A1* and *COL1A2*, respectively. The main extra–skeletal manifestations of OI include blue sclerae, opalescent teeth, and hearing impairment. Moreover, multiple genes involved in osteoblast maturation and type 1 collagen biosynthesis are now known to cause recessive forms of OI. In this study a multiplex consanguineous family of two affected males with OI was recruited for genetic screening. To determine the causative, pathogenic variant(s), genomic DNA from two affected family members were analyzed using whole exome sequencing, autozygosity mapping, and then validated with Sanger sequencing. The analysis led to the mapping of a homozygous variant previously reported in SP7/OSX, a gene encoding for Osterix, a transcription factor that activates a repertoire of genes involved in osteoblast and osteocyte differentiation and function. The identified variant (c.946C > T; p.Arg316Cys) in exon 2 of *SP7/OSX* results in a pathogenic amino acid change in two affected male siblings and develops OI, dentinogenesis imperfecta, and craniofacial anomaly. On the basis of the findings of the present study, *SP7/OSX*:c. 946C > T is a rare homozygous variant causing OI with extra–skeletal features in inbred Arab populations.

Keywords: osteogenesis imperfecta, dentinogenesis imperfecta, craniofacial anomalies, conductive hearing loss, SP7/OSX gene, consanguinity

Lay Summary

We present a multiplex consanguineous Arabian family living in Kuwait having two male siblings with a medical history of recurrent bone fractures because of bone fragility with low bone mineral density, suspected to be osteogenesis imperfecta (OI). Genetic screening revealed that both patients inherited a homozygous missense mutation of SP7/OSX, encoding Osterix, a transcription factor involved in osteoblast and osteocyte differentiation and function. Clinical and molecular investigation confirmed that this inherited mutation results in OI, dentinogenesis imperfecta, and craniofacial anomalies with late–onset unilateral hearing impairment in the two affected male siblings.

Received: November 28, 2023. **Revised:** February 15, 2024. **Accepted:** February 20, 2024
© The Author(s) 2024. Published by Oxford University Press on behalf of the American Society for Bone and Mineral Research.
This is an Open Access article distributed under the terms of the Creative Commons Attribution Non-Commercial License (https://creativecommons.org/licenses/by-nc/4.0/), which permits non-commercial re-use, distribution, and reproduction in any medium, provided the original work is properly cited. For commercial re-use, please contact journals.permissions@oup.com

Graphical Abstract

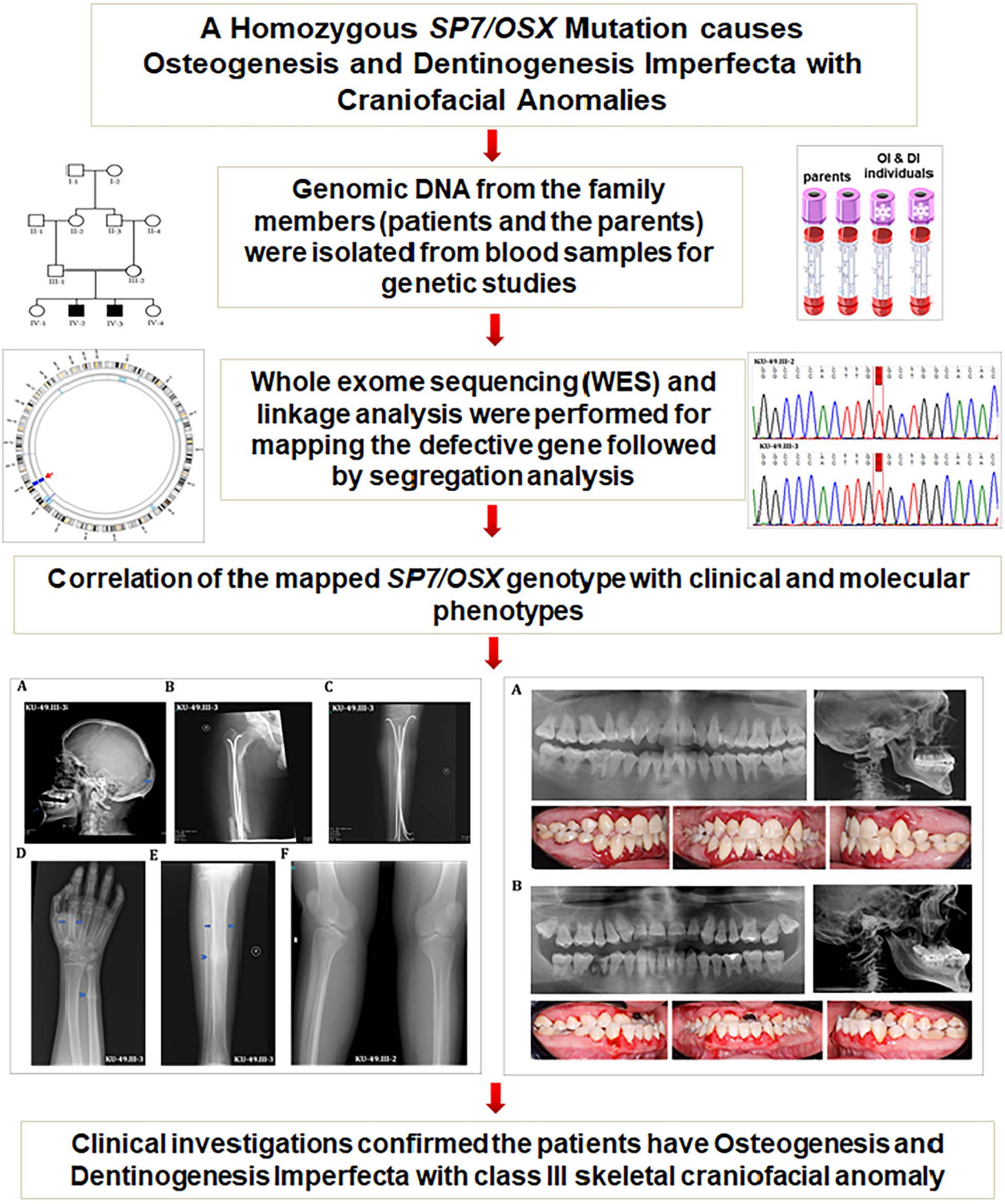

Introduction

The term osteogenesis imperfecta (OI) was originally used to describe an early onset group of connective tissue disorders that represent the most common cause of bone fragility with low mineral density (BMD). It includes various quantitative and qualitative defects of type 1 collagen and non–collagenous matrix proteins, leading to decreased production and/or defective processing of type 1 collagen, eventually leading to impaired bone strength [1, 2]. The incidence of OI is 1 in 13 500-15 000 births [3]. The classification of OI is based on the clinical phenotype: type I being the less severe, type II lethal perinatally or shortly after birth. Type III, the most severe surviving form of OI, leads to extreme disability, morbidity, and mortality. Types IV-VII of OI lead to intermediate severity. Increasingly, molecular genetics has informed this clinical classification system: specific mutations are associated

with skeletal phenotypes predicted by the affected genes and amino acids [4, 5].

Approximately, 85%-90% of cases are inherited in an autosomal dominant manner and are caused by mutations in two structural genes: the *COL1A1* (MIM 120150) encoding α1 chain and *COL1A2* (MIM 120160) encoding α2 chain. Type 1 collagen is the most abundant type of collagen in the bone matrix and is composed of two α1 chains and one α2 chain. OI also develops because of defects in several other proteins involved in the normal processing of type 1 collagen such as genes encoding proteins involved in the proper folding of the triple helix of collagen (type I). There are several extra–skeletal manifestations such as blue/gray sclera, dentinogenetic imperfecta, joint hypermobility, abnormal callus formation (type V), hearing impairment, cardiovascular and CNS complications, dentinogenesis imperfecta, and tooth eruption delay. The spectrum of severity in OI is broad and ranges from neonatal death with multiple fractures, particularly of the ribs, to patients who present in middle age with mild osteopenia and only isolated fragility fractures [1, 6]. Type I collagen is the most abundant protein initially produced by osteoblasts in the endoplasmic reticulum as a precursor molecule, type 1 procollagen, which undergoes significant modifications. The procollagen chains are mostly modified immediately post-translation and before forming the trimeric chain and these changes are important to allow for proper fibril formation. A number of different proteins and genes are implicated in this process, and relevant genetic defects have been shown to cause an OI phenotype [7-9].

Two main genes encoding for transcription factors control osteoblast differentiation; *RUNX2* (CBF-alpha-1) encodes a key transcription factor regulating the first step of osteoblast differentiation by controlling the conversation of skeletal stem cells into preosteoblasts. *Osterix* (*SP7/OSX*) encodes another transcription factor that acts early in the mesenchymal lineage, downstream of RUNX2, to promote osteoblast differentiation. Mutations in *RUNX2 (CBF-alpha-1)* and *Osterix (SP7/OSX)* genes lead to severe skeletal fragility because of osteoblast defects [6, 10, 11]. *SP7/OSX* (MIM 606633) located at 12q13.13 encodes for transcription factor Osterix which has three tandem zinc–finger motifs for DNA–binding domains. It belongs to the SP-family of protein transcription factors [12]. It is mainly involved in skeletal morphogenesis by controlling the differentiation of preosteoblast cells into terminally differentiated osteoblasts. Mutations in *SP7/OSX* cause skeletal fragility through multiple mechanisms involving cells in the osteoblast lineage [13, 14].

In null *Sp7/Osx* murine embryos, bone formation is absent because of a complete lack of osteoblasts differentiation [12]. In addition to its key roles in early lineage commitment of skeletal stem cells into osteoblasts, Osterix acts throughout the osteoblast lineage to control the expression of other osteoblast markers such as osteocalcin, osteonectin, osteopontin, and bone sialoprotein [12, 15]. Osterix also increases the expression and activity of connexin 43, a gap–junction protein that regulates intercellular communication in osteoblastic function [16]. Furthermore, *SP7/OSX* plays a crucial role in promoting maturation of osteoblasts into osteocytes, and is critical for development and maintenance of the osteocyte dendrite network [17]. In summary, the main function of *SP7/OSX* is osteoblast differentiation and maturation during embryonic bone formation [14], control of bone remodeling to ensure bone tissue turnover for maintaining bone mass [14], regulation of chondrocyte differentiation and maturation [18].

Here, we present a multiplex Arabian family in Kuwait with two affected male siblings suspected to carry a hereditary mutation causing OI with early childhood bone fragility and deformity. Autozygosity mapping followed by WES analysis led to identification of homozygous missense variant (c.946C > T; p.Arg316Cys) in exon 2 of *SP7/OSX* gene. This genetic variant is believed to be pathogenic and underlies the radiological and audiological observations typical of OI as described below.

Materials and methods

Human subjects and clinical history

Ethical approval for this project was obtained from Kuwaiti Ministry of Health Research Ethics Committee (Ethics ID: 62/2013) and it was performed with the permission of all participating family members; informed written consent was obtained from adult participants for collection of blood samples from the patients and non–affected parents. The two affected male siblings under study (KU-49.IV-2 and KU-49.IV-3) were born in Kuwait to a consanguineous, multiplex Kuwaiti family (Figure 1A) believed to be originally descended from Arabian Peninsula.

Radiological data were collected for the KU-49.IV-2 and KU-49.IV-3 patients to estimate the clinical severity of the hereditary variant on the skeletal system. Radiological findings for the two patients exhibited mandibular prognathism and wormian bones, osteopenia, fragile bones with recurrent bone fractures of the long bones secondary to minor traumatic injuries. The two patients (KU-49.IV-2 and KU-49.IV-3) were also found to have dentinogenesis imperfecta and skeletal class III deformity with midface hypoplasia. Furthermore, audiological evaluation demonstrated that KU-49.IV-2 has normal hearing and KU-49.IV-3 patient has right normal hearing and left moderately severe late onset conductive hearing loss.

The two affected male siblings had been referred for genetic assessment to clinics run by the Ministry of Health, with medical histories as follows. Proband 1 (KU-49.IV-2), born in 2000 had a significant history of low trauma fractures. At the age of 11, he sustained a fracture of the middle third of the right femur after jumping from the stairs at home and falling. The fracture was managed with closed reduction with elastic nails. At the age of 13, he developed a left femur shaft fracture when tackled during a football game. This fracture also required elastic nail fixation. His height at the age of 23 was 163 cm, his weight 86.7 kg, and his BMI 32.6.

Proband 2 (KU-49.IV-3), born in 2002, also had a significant history of fractures following low–impact trauma. At the age 11, he sustained a middle third fracture of the left femur after falling at home. The fracture required surgical intervention with double elastic nail fixation. Then, in the same year he developed a double bone fracture of the right tibia, which was managed surgically. The right tibia was fixed with four elastic nails. A year later, he developed pintract infection, so he was admitted again for elastic nail removal and debridement; one of the four elastic nails was removed from the right tibia. At the age of 13, proband 2 fell again and sustained a right femur shaft fracture. This fracture also required surgical management with elastic nailing. At the same

age, he also developed a right distal third ulnar fracture after a minor fall at home. This fracture was treated conservatively. His height at the age of 21 was 173 cm and his weight 100 kg with a BMI of 33.4.

Genomic DNA and exome sequencing

Genomic DNA was extracted from whole blood using the QIAamp mini–isolation kit (Qiagen, Hilden, Germany); concentrations were determined by UV spectrophotometry using a Nanodrop N1000 (Nanodrop Technologies Inc., Wilmington, DE, United States). Exome sequencing of genomic DNA was performed for the two patients highlighted in the pedigree, Figure 1A. Target enrichment was performed, following manufacturer's protocols, using SureSelect hybridization capture reagents with v6-capture (Agilent Technologies, Santa Clara, CA, United States). Enriched library preparations were sequenced on HiSeq 2500 platform (Illumina, San Diego, CA, United States). Linkage analysis using exome data was performed using pipeline–produced variant call format files.

Autozygosity mapping and variant screening

Genetic screening using autozygosity mapping was performed as described previously [19, 20]. Initially, AgileMultiIdeogram software (version 3) was used to visualize the homozygous intervals using exome data for linkage in which all the homozygous intervals are displayed against a circular ideogram for the 22–autosomal chromosomes for the relative patients [21]. The reference of genome annotation used was Human Genome Build hg19 (UCSC genome browser). After that, multiple linkage analysis was performed for exclusive shared identical by descent (IBD) intervals using AgileVCFMapper software (version 3), designed for viewing the autozygous intervals and determining the size IBD intervals for each chromosome using the genotypes of exome data [22]. Consequently, it was used to estimate the overlapping homozygous concordant variants shared between the two affected siblings, as seen in Figure 1C [19, 20].

Primers for variant confirmation and segregation analyses were designed using Primer3 software (http://frodo.wi.mit.edu/primer3/). The exon sequences were obtained from the University of California, Santa Cruz Genome Browser (http://genome.ucsc.edu/) for exon 2 of *SP7/OSX* gene. The sequence of the forward primer used was "5´-CTACCCAGCTCCCCACCTCT-3´" and the sequence of the reverse primer was "5´-TCCGAACGAGTGAACCTCTT-3´." All targets were amplified using a commercial PCR master mix (Promega, Southampton, United Kingdom). PCR was performed in a total reaction volume of 20 μl. The master mix contained 4 μl of 5x Flexi buffer, 1.2 μl of 25 mM $MgCl_2$, 0.4 μl of 10 mM dNTP that contained a mixture of dATP, dCTP, dGTP and dTTP nucleotides and 1.2 units of TaqFlexi DNA polymerase. The amount amplified was 40 ng of genomic DNA. For all amplicons, initial denaturation was at 95°C for 30 s, followed by 30 cycles of 95°C for 15 s, 58°C for 15 s, 72°C for 30 s and a final 300 s extension at 72°C. Amplicons were purified by using ExoSAP-IT exonuclease (USB Corporation, Cleveland, United States) according to the manufacturer's instructions. PCR products were stained by ethidium bromide and separated on a 1.5% agarose gel. Sequencing was performed using the BigDye 3.1 kit (Applied Biosystems, Foster City, United States). Sequencing reactions were ethanol-precipitated and resuspended in HiDi formamide (Applied Biosystems, Foster City, United States) before analysis on a 3130xl genetic analyzer with a 36 cm capillary array. The Sanger sequencing results were analyzed using a GeneScreen software [23].

Patients' evaluation for dentinogenesis imperfecta and craniofacial anomalies

The two affected siblings KU-49.IV-2 and KU-49.IV-3 were referred to Craniofacial Orthodontist at the Cleft and Craniofacial Unit, Farwaniya Specialized Dental Center, for intraoral and extraoral examination of the dental and craniofacial skeletal anomalies. Photographs were obtained using Canon 250D Camera, with a 100 mm lens. Cone Beam Computed Tomography was taken using an iCAT flex machine with a 23 × 17 field of view. Panographic and cephalometric radiographs were exported using QuickCeph Studio Software (5.2.2). Dental history was collected through examination and patient interview.

Patients' evaluation for hearing impairment

KU-49.IV-2 and KU-49.IV-3 were further referred firstly to an audio–vestibular physician and then to an ENT consultant for a full audiological evaluation, which comprised five different tests as detailed below: the first auditory test was the Pure Tone Audiogram, a behavioral test used to measure hearing sensitivity. This test involves the peripheral and central auditory systems [24] and measures the pure–tone thresholds that indicate the softest sound audible to an individual at least 50% of the time. Hearing sensitivity is plotted on an audiogram displaying intensity as a function of frequency [24]. The second auditory test was tympanometry, which provides a graphic representation (tympanogram) for the movements of eardrum in response to the air pressure in the ear canal [24]. The third test was the Acoustic reflex, which measures the response of the intratympanic muscles to high sound pressure [24]. The fourth test was for otoacoustic emissions (OAE), sounds generated from the cochlea and transmitted across the middle ear to the external ear canal, where they can be recorded [24]. The fifth auditory test was the auditory brainstem response (ABR), used to detect hearing loss by measuring the brain's response to sound [24].

Results

Autozygosity mapping reveals a homozygous missense variant in SP7/OSX

The two patients KU-49.IV-2 and KU-49.IV-3 were suspected to carry disease–causing hereditary variants as more than one individual exhibited the same phenotype (Figure 1A). Therefore, genetic studies were performed for the two siblings to confirm the OI diagnosis; affected family members showed clinical features typical of the hallmark disease of OI (MIM: 606633), including bone fragility, bone deformity, growth deficiency, low bone density, with high susceptibility to fracture from minimal trauma [25, 26].

Linkage analysis using an autozygosity mapping approach was performed for the two affected individuals (Figure 1B). The resolution of linkage analysis using exome data was further increased by using higher v6-capture that covers bigger regions of noncoding sequence (61 Mb) compared with the standard v7-capture (37 Mb). The use of v6-capture increases the level of detection of the smaller IBD intervals

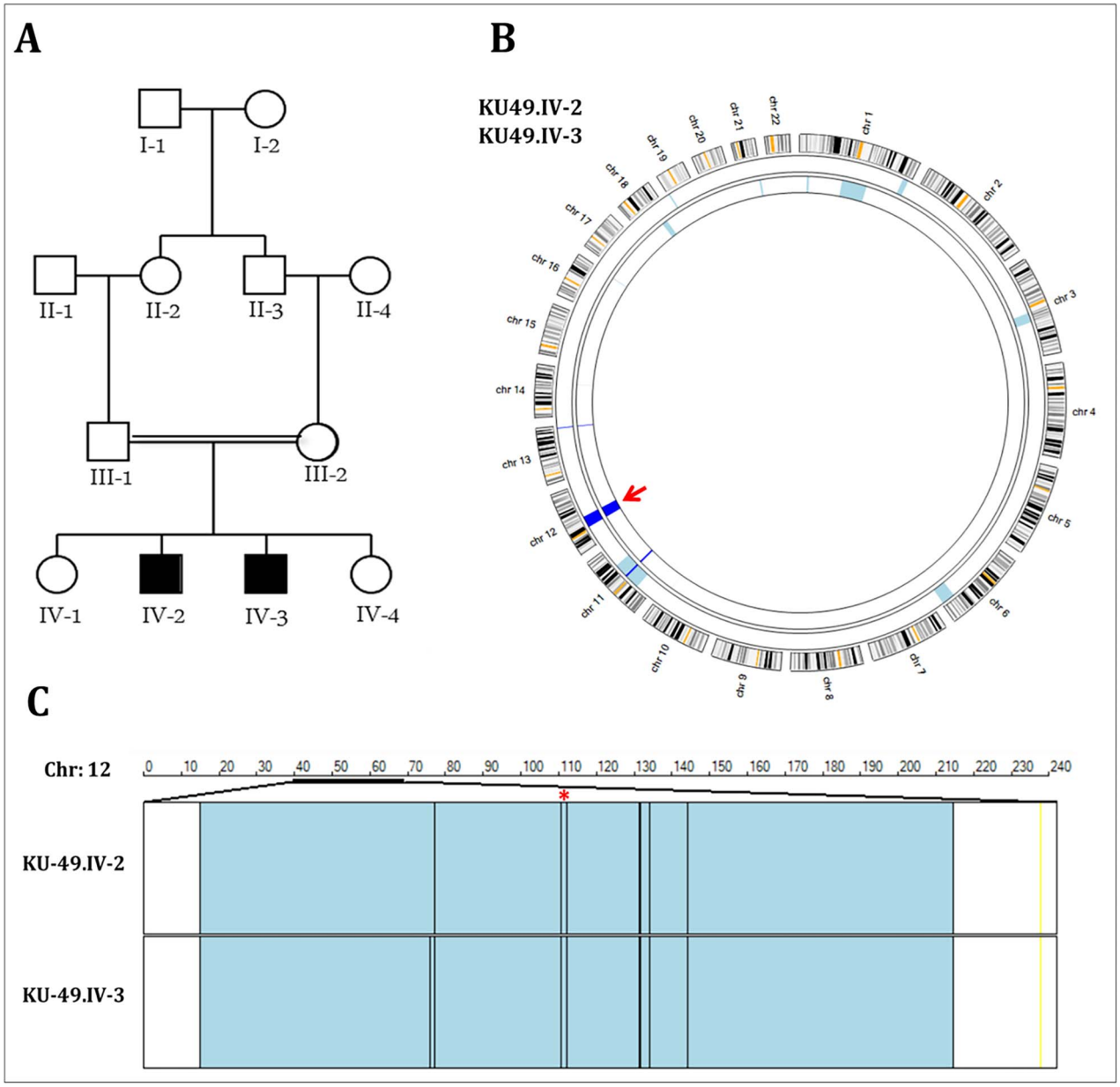

Figure 1. Genetic linkage of 22-autosomal chromosomes of Family KU-49. Figure 1A shows the pedigree of Family KU-49, which has two affected male siblings with OI (KU-49.IV-2 and KU-49.IV-3). Figure 1B is the Agile Multi Ideogram for the two affected male siblings that indicates a significate shared IBD interval at chromosome 12, highlighted by a red arrow. The ideogram is representing the linkage scan as circular axis for the KU-49.IV-2 and KU-49.IV-3 OI individuals belonging to the same family in one group. In multiplex families: the exclusive regions of homozygosity (ROH) shared between the affected relatives are displayed as navy-blue bars. The homozygous regions that are not shared among affected relatives are displayed as light blue bars. As seen from the initial linkage scan the two patients have shared IBD intervals (navy blue bars) at chr:11, chr:12 and chr:13. The two affected siblings have only one exclusive shared IBD at chr: 12 across the *SP7/OSX* locus indicated by a red arrow. In the ideogram the linkage scan is presented from the ideogram edge (first circus: KU-49.IV-3) towards the centre (last circus: KU-49.IV-2). The alignment is solely controlled by the software. Figure 1C Multiple linkage analysis at chromosome 12 for the two affected siblings that performed using AgileVCFMapper software. The shared IBD interval at chr: 12 was estimated to be (41,454,063-65,805,469). The physical location of SP7/OSX is at Chr12: 53,326,575-53,336,354 (within the estimated IBD interval) and highlighted by the red asterisk. As seen, each row represents the genotypes for chromosome 12 for one OI individual. The concordant autozygous shared and common alleles represented as (blue lines); concordant autozygous rare alleles that most likely harbouring rare pathogenic variants represented as (black lines); homozygous discordant alleles represented as (yellow lines).

and gives better resolution for linkage. Mapping these shared IBD intervals is the key for disease–gene identification in patients belonging to multiplex families. The width of the IBD interval represents the extent of the autozygous regions [21, 27]. The results showed a unique autozygous interval (blue bar) at chromosome 12 across the *SP7/OSX* locus shared between the two affected siblings and highlighted by red arrow (Figure 1B). Multiple linkage analysis was performed at chromosome 12 using AgileVCFMapper software [22]. The shared IBD interval at chr: 12 was precisely estimated to be (41454063-65805469) around 24 MB. The physical location of *SP7/OSX* is at Chr12: 53326575-53336354 (within the estimated IBD interval), as seen in Figure 1C. Subsequent analysis of exome data at the shared IBD interval revealed a homozygous variant (c.946C > T; p.Arg316Cys) in exon 2 of *SP7/OSX* gene. Sequencing chromatograms of the two

affected siblings and their parents confirmed that KU-49.IV-2 and KU-49.IV-3 harbor this homozygous missense variant detected in *SP7/OSX* and segregated with the disease phenotype (Figure 2).

We used in silico analyses to predict the pathogenicity of *SP7/OSX*: c.946C > T using the top five features of mutation prediction tools. First, the loss of molecular recognition features (MoRFs) binding score was measured; this estimates the pathogenicity of the variant specifically at susceptible segments of the protein that exhibit molecular recognition and binding functions. Loss of MoRF binding (P = .003), indicating a significant loss of function [1, 2]. Loss of methylation at p.Arg316 (P = .0718) is an important epigenetic mark that estimates the allelic expression of imprinted genes. Genomic imprinting is a process of gene silencing by DNA methylation [3, 4]. Since the silenced allele is methylated, whereas the active allele is unmethylated, a P-value > .05 is typically considered to represent a variant in a hypermethylated state [5]. The structural and functional effects of amino acid substitutions were statistically estimated to predict the effect of the variant on the protein in 3D structures and in the development of a genetic disease. These so–called functional residue predictors then quantify the impact of disease–causing amino acid substitutions on catalytic activity [6]. In addition, *SP7/OSX*: c.946C > T has a gain of catalytic residue at Trp 317 (P = .0732), loss of disorder (P = .0754), and loss of helix (P = .1299), all of which are consistent with the variant being highly damaging [7, 8]. In conclusion, the overall score results suggest that *SP7/OSX*: c.946C > T has significantly altered the protein structure and function by disrupting the stability of 3D structures [9]. As previously reported, the deleterious allele located in putative sequence and alter the alpha helix of the first zinc finger domain [10].

Furthermore, eight metatools are available in the dbNSFP database, developed for the annotation and functional prediction of all potential non–synonymous single–nucleotide variants in the human genome. All determine pathogenicity based on the combined evidence from several other in silico predictors and all predict *SP7/OSX*: c.946 C > T to be deleterious/pathogenic/deleterious and disease-causing; MetaLR (0.1761), MetaSVM (-0.7308), REVEL (0.681), DANN (0.999380376), MutPred (0.91508), Mutation assessor (2.805), MutationTaster (0.81001), Provean (-7.84), and Polyphen-2 (1) [11-13].

The radiological findings showed that the two OI affected siblings exhibit many of the traits seen in the nonlethal form of the OI, including mandibular prognathism and wormian bones (Figure 3A) as well as osteopenia and unusually fragile bones. As a result, they frequently presented to the ED because of repeated fractures of the long bones secondary to minor traumatic injuries, which often required surgical management, as seen in Figure 3B and C.

Radiographs of the forearm show a broad configuration (metaphyseal flaring) giving the appearance of a subtle Erlenmeyer flask deformity of the metacarpal (arrowheads, Figure 3D), and a transverse lucent line at the distal diaphysis of the ulna surrounded by solid periosteal reaction consistent with callus formation (healed recent fracture, Figure 3D). Leg radiographs show a broad configuration of the midshaft of the right tibia associated with a thin sclerotic transverse line and surrounding solid periosteal reaction on both sides of the tibia consistent with healed old fractures (Figure 3E, arrowheads). Walking difficulty because of genu valgum deformity was also seen in patient KU-49.IV-2 (Figure 3F).

Regarding dental and craniofacial anomalies, for the KU-49.IV-2 patient (Figure 4A), examination of the craniofacial region revealed class III skeletal tendency because of retruded maxilla and protruded mandible, with Stahl's ears deformity. Intraorally, he presents with Class III dental relationship, moderate–severe crowding in the upper and lower arches, and minimal overjet and overbite. Poor oral hygiene and multiple carious lesions were identified; scaling was carried out and revealed opalescent and slightly brown lower and upper molars. Panoramic radiograph shows short roots, obliterated canals, and bulbus crowns with conical constriction associated with dentinogenesis imperfecta type I. He also reports witnessed sleep apneas and scored high on the Epworth Sleepiness Scale. He was referred to the general dentist and sleep specialist before planning any orthodontic intervention.

The KU-49.IV-3 patient (Figure 4B) presented with a concave profile, severe class III skeletal discrepancy because of retruded maxilla and protruded mandible, and a high mandibular plane angle. Upon intraoral examination, moderate crowding in the upper and lower arches was documented in addition to anterior and posterior crossbite, with a -8 mm overjet and 2 mm of overbite. His upper and lower teeth presented with opalescent and slightly brown appearance, especially on the buccal surface of the upper molars. Panoramic radiographs also revealed short roots, obliterated canals, bulbus crowns with conical constriction associated with dentinogenetic imperfecta type I. Similar to his sibling, he presents with poor oral hygiene, multiple carious lesions, and a moderate score on the Epworth Sleepiness scale. Referrals to the general dentist and sleep specialist took place before proceeding with any orthodontic/surgical intervention.

A full audiological evaluation performed at Zain Hospital ENT Clinic showed that the KU-49.IV-2 individual's hearing is normal, whereas KU-49.IV-3 has a left ear conductive hearing loss. The results of the auditory tests for KU-49.IV-3 are summarized in Table 1.

A CT scan was then performed on patient KU-49.IV-3 to assess the integrity of the ossicles and to determine if there was any abnormal ossification. The results showed bilateral ill–defined areas of bony lucency just anterior to the oval windows in the region of the fissula ante fenestram, consistent with the otospongiotic phase of otosclerosis (Figure 5). The remaining structures, including the ossicles and middle ear fissures, were unremarkable, ruling out a congenital defect in the ossicles and inner ear structures, and suggesting that the adult–onset unilateral hearing loss is most likely because of an early stage defect in bone remodeling of the stapes footplate bone, which is not visible. The audiologist recommended regular follow-up for early detection of expected conductive hearing loss in the right ear. It was also suggested to proceed with either stapedectomy or hearing aid use if the patient has a hearing loss in the right ear. It is also recommended that the KU-49.IV-2 individual undergo regular hearing tests at least once a year, as he has a high probability of developing hearing impairment.

Discussion

Here we report the mapping of a disease–causing variant in *SP7/OSX* gene in two affected siblings with OI, a rare autosomal recessive disorder, using autozygosity mapping [28-30].

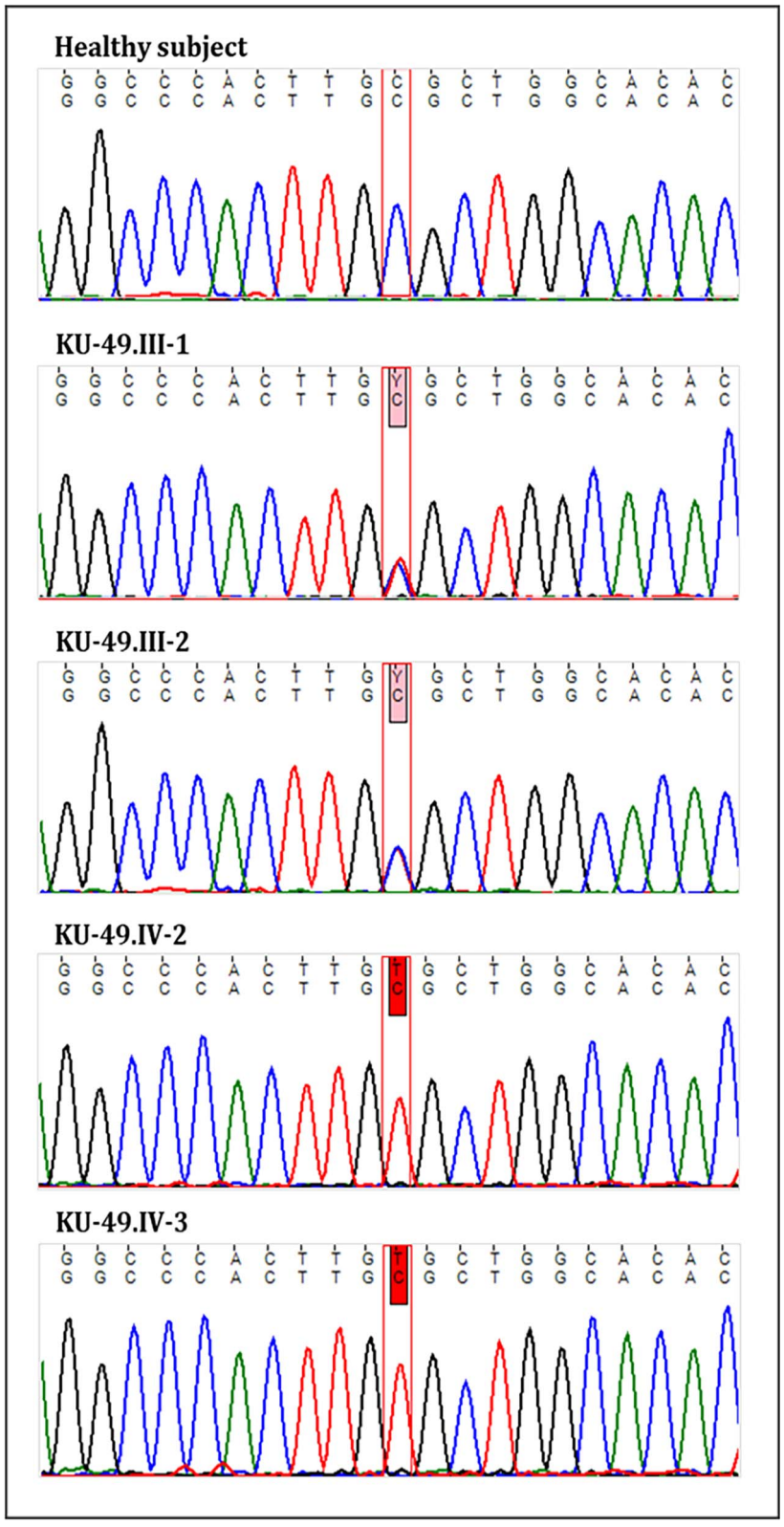

Figure 2. *SP7/OSX* variants chromatographs for the members of family KU-49. The figure represents the sequences for the healthy subject, the parents (KU-49.III-1 and KU-49.III-2), and the two OI patients (KU-49.IV-2 and the KU-49.IV-3), respectively. The two affected siblings KU-49.IV-2 and KU-49.IV-3 carry a homozygous missense variant (c.946C > T; p.Arg316Cys) in exon 2 of *SP7/OSX* that results in an arginine to cysteine amino acid change. This variant has no RS number to date. Segregation analysis demonstrate that the parents, KU-49.III-1 and KU-49.III-2, are heterozygous carriers for this variant consistent with the fact that this variant is segregated with OI phenotype in this family compared with the healthy subject that carries the two normal wild–type alleles. The MedPred = 0.81, which indicates the variant is very damaging.

Figure 3. Main radiological findings for the two affected siblings KU-49.IV-2 and KU-49.IV-3. (A) Lateral radiograph of the skull of the KU-49.IV-3 patient demonstrates type III dental malocclusion with mandibular prognathism (line arrow) and wormian bones (block arrow) with occipital protuberance. (B) Radiograph of the proximal right femur of the KU-49.IV-3 patient shows an insuffiency spiral fracture, which was managed gamma nails. (C) Radiograph of the right leg of the KU-49.IV-3 patient demonstrating a healing fracture of the tibia with intramedullary fixation nails in situ. (D) Radiograph of the forearm of the KU-49.IV-3 patient shows undertublation of the meatacarals (block arrows) with healing fractures demonstrated in the ulna (chevrons). (E) Radiograph of the leg of the KU-49.IV-3 patient show undertublation of the tibia (block arrows), with healing fractures demonstrated tibia (chevrons). (F) Knees radiograph of the KU-49.IV-2 patient shows diffuse osteopenia with genu valgum deformity with lower leg bending outwards with respect to the long axis of the femur.

Table 1. A full audiological evaluation for KU-49.IV-3 individual that confirmed a left moderately severe conductive hearing loss.

Auditory tests	Clinical findings for KU-49.IV-3 individual
Puretone audiogram	Right within normal hearing (Figure S1A) and left moderately severe conductive hearing loss (Figure S1B).
Tympanometry and acoustic reflex	Bilateral type (A) (Figure S2A); absent both ipsilateral and contralateral reflexes (Figure S2B and C).
Speech audiometry	Bilateral excellent speech discrimination clinical evaluation by audiologist.
OAE	Right pass emission (Figure S3A) and left failed emission (Figure S3B).
ABR test	ABR waveforms were repeatable, identifiable, and recordable down to 30 dB nHL in the right side (Figure S4A) and down to 40 dB nHL in the left side (Figure S4B) with delayed absolute latencies of wave V (Figures S4B and S5).

A wide variety of skeletal phenotypes have been associated with *SP7/OSX* variants [13], ranging from low bone density because of common noncoding variants to severe skeletal dyscrasias from dominant point mutations [31]. Previous studies on *SP7/OSX* have been shown to cause OI type XII. Pathogenic variants in *SP7/OSX* were previously reported by

Figure 4. Intraoral photographs and dental radiographs confirming the two patients have dentinogenesis imperfecta and craniofacial anomalies: panoramic and cephalometric radiographs for the two affected siblings: (A) KU-49.IV-2 and (B) KU-49.IV-3. The clinical evaluation was clearly explained in the results section.

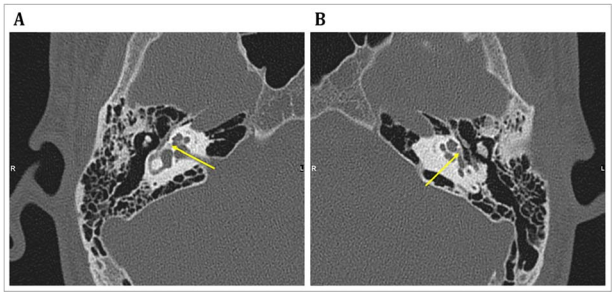

Figure 5. Hight resolution CT scan of the petrous bones for KU-49.IV-3 patient. It shows ill–defined lucency (focal demineralization) in the region of the fissula ante fenestrum bilaterally (arrows). Cochlea and the ossicles are spared. Findings consistent with bilateral otosclerosis (fenestral type): (A) right and (B) left.

Lapunzina et al. [13] in an 8–year–old Egyptian boy with a recessive type of OI. He inherited a loss–of–function variant (c.1052delA; p.Glu351GfsX19) that causes premature termination of translation and the truncated protein lacks the last 81 amino acids. This mutation generates 18 new amino acid residues downstream of codon 351, resulting in the absence of the third domain of the zinc finger. The clinical findings of this patient were multiple fragility fractures, mild bone deformities including bowing of the upper and lower limbs, mild scoliosis, delayed tooth eruption, and low BMD in the lumbar spine and femur. Normal alkaline phosphatase indicated normal bone turnover. Craniofacial anomalies included mild facial dysmorphism, high forehead with prominent supraorbital ridges, midface hypoplasia, depressed nasal bridge, microstomia, micrognathia, and high arched palate. Delayed dental eruption was noted, with no dentinogenesis imperfecta. His hearing and sclerae were normal [13]. Another case report study by Tung et al. [32] presented a 17–year–old Chinese boy diagnosed with OI type XII carrying the same homozygous frameshift mutation in *SP7/OSX* (c.1052delA; p. Glu 351GfsX19). The main clinical manifestation was recurrent long bone fractures with vertebral collapse. He had also undergone repeated orthopedic surgery, including corrective osteotomy of the left tibia and modified Sofield procedures of the bilateral tibiae. Delayed DI, primary dentition, enamel hypoplasia, discolouration, obliterated pulp chamber, permanent dentition, bulbous crowns, and short roots were noted [32].

Another study on recessive OI was presented by Hayat et al. [33] on a 32–year–old Pakistani man with a negative history of OI but who had multiple fractures since birth. His weight and height were 30 kg and 95 cm, respectively. Physical examination revealed bilateral bowing of the extremities mainly femur, tibia and fibula, severe scoliosis, short stature, with canonical dysmorphism. He had normal hearing and sclera without dentinogenesis imperfecta. Genetic screening revealed that the patient had a homozygous missense mutation in the *SP7/OSX* gene (c.824G > A; p.Cys275Tyr) resulting in no

change in the three zinc finger domains. Structural modeling of the p.Cys275Tyr mutant showed an inability of the secondary structure of Osterix to interact with other bone transcription factors, mainly Runx2 and Dlx5, which are involved in osteoblast differentiation [33].

Fiscaletti et al. [1] reported a 13–year–old Iraqi male carrying a homozygous pathogenic missense variant (c.946C > T; p.Arg316Cys) in *SP7/OSX*, which is the same mutation mapped in our study of the two affected males. It was reported to cause recessive OI and to alter the first zinc finger domain. Clinical examination revealed a low–trauma femur fracture, short stature, mild scoliosis, craniofacial anomalies with late onset hearing impairment. Bone biopsies showed significant cortical porosity and high trabecular bone turnover. BMD at the lumbar spine had been low since childhood [1].

A recent study by Ludwig et al. [34] described a rare case with late onset of dominant OI in a 20–year–old Haitian man carrying a heterozygous missense mutation in *SP7/OSX* (c.1019A > C; p.Glu340Ala) affecting a highly conserved consensus sequence in the second zinc finger domain. The main clinical manifestations include multiple fragility fractures mainly of the long bone diaphysis, poor fracture healing, severe scoliosis, and low cortical volumetric BMD. Bone histomorphometry showed thin cortices and low bone turnover with reduced osteoblast function, although all previously reported patients with *SP7/OSX* mutations have high bone turnover. The patient had fractured teeth and malocclusion without DI and facial malocclusion. Cortical bone porosity and low cortical density was consistent with previously reported OI individuals with *SP7/OSX* mutations. Dual luciferase reporter assay using co–transfected plasmids carrying the mutant *SP7/OSX* with *DLX5* showed a significant reduction in the transcriptional luciferase activities of co–transfected plasmids compared with wild–type *SP7/OSX* [34].

A study by Whyte et al. [35] of a 15–year–old Caucasian female reported a de novo heterozygous missense mutation (c.926C > G; p. Ser309Trp) in *SP7/OSX* causing Juvenile Paget's disease by altering the first zinc finger domain. The patient had a history of atraumatic fracture of the long bones of the lower extremities as an infant, mild scoliosis with cortical thickening, and skull deformity with facial dysmorphism. She also had generalized osteosclerosis and hyperostosis and developed a mild sensory hearing loss. Dental examination for tooth morphology and eruption showed DI, short roots, with thin, or no pulp. Biochemical studies were consistent with a positive mineral balance and several markers of bone turnover were elevated, including a marked hyperphosphatasemia. Bone histopathology of the iliac crest was consistent with rapid skeletal remodeling. Measles virus transcripts, common in classic Paget's disease of bone, were not detected in circulating mononuclear cells [35].

This same de novo dominant neomorphic missense variant (c.926 C > G: c.926C > G; p. Ser309Trp) in *SP7/OSX* was found by Lui et al. [31] in a 3–year–old Caucasian boy with a complex skeletal disorder including severe scoliosis, long bone fragility, craniosynostosis, cranial hyperostosis, increased bone density with thickened intramembranous bones, and decreased bone density in other areas. Bone histomorphometry revealed increased osteoblast numbers and increased osteoid, but decreased osteoid mineralization, suggesting impaired osteoblast–mediated osteoid mineralization. An in vivo study in mutant mice carrying the same neomorphic variant showed that the variant altered the DNA binding specificity of Osterix, resulting in decreased binding of Osterix to DLX proteins. The variant shifted the binding specificity of Osterix from AT–rich motifs to a GC consensus sequence, which is critical for normal osteoblast differentiation. Mutant mice with the corresponding variant also show a complex skeletal phenotype that differs from that of Sp7 null mice, suggesting the pathogenicity of the heterozygous variant in *SP7/OSX* [31].

In terms of clinical phenotypes, both patients we report here presented with similar skeletal class III deformity and midface hypoplasia, consistent with the previous findings of the Lapunzina et al. [13] and Fiscaletti et al. [1] studies, the latter reporting a similar medical history of low–impact fractures, craniofacial abnormalities, irregular dental features, and progressive hearing loss. OI–like skeletal fragility in patients who were siblings in an Iraqi family with a tradition of consanguineous marriage found to have the same *SP7/OSX* (c.946C > T; p.Arg316Cys) mutation as reported here. However, in terms of differences from earlier studies, our subjects KU49.IV-2 and KU49.IV-3 were diagnosed with dentinogenesis imperfecta through radiographs and clinical examination, whereas the sole dental problem of the cases reported by Fiscaletti et al. [1] and Lapunzina et al. [13] was delayed eruption, with both reporting the absence of dentinogenesis imperfecta. Furthermore, the two siblings (KU-49.IV-2 and KU-49.IV-3) report irregular dental visits, as evident in the presentation of poor oral hygiene, inflamed gingiva, and the multiple carious lesions. Periapical lesions on the lower right first molar in both siblings were noticed. Severe gingival inflammation was noticed with accumulated calculus, which was removed prior to documentation. Removing such calculus revealed the discoloration, which was vital to the dentinogenesis imperfecta diagnosis. Both cases were referred to the general dentist for scaling and placed on 3 months recall appointment system. Oral hygiene instructions were reviewed and the importance of following them at home was emphasized.

Fiscaletti et al. [1] additionally reported short stature and other spinal abnormalities in their patients. Similarly, craniofacial dysmorphisms was described by Hayat et al. [33], Ludwig et al. [34], and Whyte et al. [35]. Additional findings including fragile teeth [8] and delayed eruption with short pulp–less roots [9] were reported. On the other hand, Lui et al. [31] uniquely described craniosynostosis and cranial hyperostosis in his case report. The growth of the mandible typically continues after the end of the maxillary growth leading to an increase in the skeletal discrepancy and facial convexity. In KU-49.IV-3 and KU-49.IV-2, whose ages are 21 and 23, respectively, most of the growth had occurred, thus no significant changes would be expected.

With regard to hearing impairment, for the autosomal recessive form of OI, Lapunzina et al. [13] reported normal hearing. However, similarly to the Fiscaletti et al. [1] study, we report here that one of the affected siblings in the KU-49 family had a progressive hearing impairment. It is worth noting that the KU-49 family reported here is unrelated to the family described by Fiscaletti et al. [1]. The differences in hearing function in affected siblings might be controlled by the other genetic and environmental factors [36, 37]. It was recently reported that pathogenic variants in *SP7/OSX* are associated with hearing loss are accounted for by the fact that bone structures within the collagen rich matrix in the auditory system are vital for sound amplification and transmittance [37].

Apparently 50% of adults with dominant OI have severe sensory hearing loss because of deleterious variants in COL1A1 or COL1A2 [37, 38]. OI patients carrying pathogenic variants in *COL1A1* or *COL1A2* genes often have early onset hearing loss [39]. Similarly, patients carrying pathogenic variants in *SP7/OSX* have been previously reported to have bone fragility with hearing impairment and anatomically have abnormal ossicles and temporal petrous bones [1]. In this study, a full audiological evaluation for the two affected siblings KU-49.IV-2 and KU-49.IV-3 has shown that the KU-49.IV-2 individual has normal hearing. On the other hand KU-49.IV-3 has normal right hearing and a moderately severe conductive hearing loss in the left ear. Radiological findings confirmed KU-49.IV-3 has severe left hearing loss because of bilateral lucency of the fissula ante fenestrum that is mainly caused by defect in bone remodeling consistent with OI phenotype.

Therefore, the pathogenic variant (c.946C > T; p.Arg316Cys) in *SP7/OSX* gene is believed to be causing late onset progressive conductive hearing loss for KU-49.IV-3, mainly because of ossification of the stapes footplate of the ossicle. Although the CT scan shows normal morphology and configuration of the ossicles this might be expected to be seen in OI patients at this age (early 20s) with the degree of sclerosis being too small to be picked up by CT. However, bilateral lucency of the fissula ante fenestrum is a major indication of otosclerosis. Therefore, the identified pathogenic variant is directly involved in the development of late onset progressive hearing impairment. ENT consultation suggested late onset bilateral conductive hearing loss for the two patients under study. The function and the expression of *SP7/OSX* in nonskeletal tissue were investigated in animal models in the otic placode in Medaka and Zebrafish [40, 41]. This gene is also found to be expressed in the brain and olfactory bulb in mice [42]. Functional studies in *SP7/OSX* orthologues knockdown animal models show reduced numbers of otoliths and impairment in the formation of the sensory maculae [43]. Most of the literature indicates that the hearing losses in OI patients are late onset, mainly occurring in the second to the third decade of age [44-46]. Therefore, it is recommended to perform systematic audiology screening tests in children with OI.

The mechanisms by which Osterix promotes osteoblast differentiation are well-studied [47]. In pre-osteoblasts, Osterix cooperates with Dlx family transcription factors to regulate the enhancer regions in osteoblast–specific genes [48]. In mature osteoblasts, Osterix regulates a distinct subset of cell type–specific enhancers to promote dendrite formation and osteocyte maturation [17]. Future studies are needed to assess the impact of the (c.946C > T; p.Arg316Cys) point mutation on the distinct functions of Osterix throughout the osteoblast lineage. Osteocyte dendrite defects noted in bone biopsies from Iraqi patients suggest that this mutation may interfere with the osteocytic actions of the transcription factor [17], and $SP7^{R316C}$ shows defects in transactivating osteocyte–specific enhancer elements compared with wild–type *SP7/OSX*. The *SP7/OSX* locus was previously reported as an osteoporosis susceptibility locus in several genome–wide association studies [49-51]. Genetic polymorphisms in the *SP7/OSX* are common risk factors for low bone density in adults and children [50, 51] and also affect the rate of BMD acquisition [49].

In summary, here we describe the clinical phenotypes of additional patients having OI and dentinogenesis imperfecta with craniofacial anomaly mainly midface hypoplasia and skeletal class III deformity that bearing a hereditary homozygous (*SP7/OSX*; c.946C > T; p.Arg316Cys) mutation. This information adds to the growing body of evidence demonstrating a crucial role for this transcription factor in skeletal development and disease.

Acknowledgments

We are grateful to the OI patients and their parents for their participation in the study. We thank the Ministry of Health at the State of Kuwait for granting the ethical approval to conduct this study. We also thank Al-Razi hospital, the specialized orthopedic hospital in Kuwait for providing the cases under study. We would like to thank Dr Fatmah Alhendi, oral medicine specialist, for her valuable assistant. We also thank Dr Atef Ali Marey, audio–vestibular physician, at Zain Hospital in Kuwait for conducting full audiological evaluations for the two patients under study. We thank Jialiang Wang at Harvard Medical School for her suggestions. We thank Professor Trevor Batten at University of Leeds, United Kingdom, for his invaluable comments on the manuscript.

Author contributions

Dalal Al-Mutairi (Conceptualization, Data curation, Formal analysis, Funding acquisition, Investigation, Methodology, Project administration, Resources, Software, Supervision, Validation, Visualization, Writing—original draft, Writing—review & editing), Ali Jarragh (Investigation), Basel H. Alsabah (Investigation), Marc Wein (Writing—review & editing), Wasif Mohammed (Investigation), and Lateefa Alkharafi (Investigation). D.A.-M. designed the study, performed the autozygosity mapping, variant screening and validation, segregation analyses, prepared all the figures and wrote the manuscript. A.A.J., the orthopedic surgeon that referred the two patients for genetic screening to the Faculty of Medicine after performing surgical procedures on KU-49.IV-3 patient and obtained the informed consent. B.H.A., ENT consultant at Zain Hospital, referred the two patients for hearing assessment and performed the final hearing assessment for the two patients. M.N.W. reviewed the manuscript. W.M., radiologist at Al-Sabah hospital that provided and commented on the radiological findings for the two patients in this study. L.A.-K. is a craniofacial orthodontist who clinically examined the two patients for dental and facial skeletal anomalies, provided the clinical description and diagnosis of dentinogenesis imperfecta and craniofacial anomalies. Contributed to the review of the manuscript.

Supplementary material

Supplementary material is available at *JBMR Plus* online.

Funding

None declared.

Conflicts of interest

None declared.

Data availability

Data available on request from the authors.

References

1. Fiscaletti M, Biggin A, Bennetts B, et al. Novel variant in Sp7/Osx associated with recessive osteogenesis imperfecta with bone fragility and hearing impairment. *Bone*. 2018;110:66–75. https://doi.org/10.1016/j.bone.2018.01.031.

2. Saad FA. Novel insights into the complex architecture of osteoporosis molecular genetics. *Ann N Y Acad Sci*. 2020;1462(1):37–52. https://doi.org/10.1111/nyas.14231.
3. Tournis S, Dede AD. Osteogenesis imperfecta - a clinical update. *Metabolism*. 2018;80:27–37. https://doi.org/10.1016/j.metabol.2017.06.001.
4. Chen C, Jiang Y, Xu C, et al. Skeleton genetics: a comprehensive database for genes and mutations related to genetic skeletal disorders. *Database (Oxford)*. 2016;2016. https://doi.org/10.1093/database/baw127.
5. Rossi V, Lee B, Marom R. Osteogenesis imperfecta: advancements in genetics and treatment. *Curr Opin Pediatr*. 2019;31(6):708–715. https://doi.org/10.1097/MOP.0000000000000813.
6. Richards JB, Zheng HF, Spector TD. Genetics of osteoporosis from genome-wide association studies: advances and challenges. *Nat Rev Genet*. 2012;13(8):576–588. https://doi.org/10.1038/nrg3228.
7. Kasher M, Williams FMK, Freidin MB, et al. Understanding the complex genetic architecture connecting rheumatoid arthritis, osteoporosis and inflammation: discovering causal pathways. *Hum Mol Genet*. 2022;31(16):2810–2819. https://doi.org/10.1093/hmg/ddac061.
8. Raisz LG. Pathogenesis of osteoporosis: concepts, conflicts, and prospects. *J Clin Invest*. 2005;115(12):3318–3325. https://doi.org/10.1172/JCI27071.
9. Zaidi M. Skeletal remodeling in health and disease. *Nat Med*. 2007;13(7):791–801. https://doi.org/10.1038/nm1593.
10. Komori T. Signaling networks in RUNX2-dependent bone development. *J Cell Biochem*. 2011;112(3):750–755. https://doi.org/10.1002/jcb.22994.
11. Engin F, Yao Z, Yang T, et al. Dimorphic effects of notch signaling in bone homeostasis. *Nat Med*. 2008;14(3):299–305. https://doi.org/10.1038/nm1712.
12. Nakashima K, Zhou X, Kunkel G, et al. The novel zinc finger-containing transcription factor Osterix is required for osteoblast differentiation and bone formation. *Cell*. 2002;108(1):17–29. https://doi.org/10.1016/S0092-8674(01)00622-5.
13. Lapunzina P, Aglan M, Temtamy S, et al. Identification of a frameshift mutation in Osterix in a patient with recessive osteogenesis imperfecta. *Am J Hum Genet*. 2010;87(1):110–114. https://doi.org/10.1016/j.ajhg.2010.05.016.
14. Gao Y, Jheon A, Nourkeyhani H, Kobayashi H, Ganss B. Molecular cloning, structure, expression, and chromosomal localization of the human Osterix (SP7) gene. *Gene*. 2004;341:101–110. https://doi.org/10.1016/j.gene.2004.05.026.
15. Han Y, Cho DH, Chung DJ, Lee KY. Osterix plays a critical role in BMP4-induced promoter activity of connexin43. *Biochem Biophys Res Commun*. 2016;478(2):683–688. https://doi.org/10.1016/j.bbrc.2016.08.007.
16. Baek WY, de Crombrugghe B, Kim JE. Postnatally induced inactivation of Osterix in osteoblasts results in the reduction of bone formation and maintenance. *Bone*. 2010;46(4):920–928. https://doi.org/10.1016/j.bone.2009.12.007.
17. Wang JS, Kamath T, Mazur CM, et al. Control of osteocyte dendrite formation by Sp7 and its target gene osteocrin. *Nat Commun*. 2021;12(1):6271. https://doi.org/10.1038/s41467-021-26571-7.
18. Glorieux FH, Travers R, Taylor A, et al. Normative data for iliac bone histomorphometry in growing children. *Bone*. 2000;26(2):103–109. https://doi.org/10.1016/S8756-3282(99)00257-4.
19. Al-Mutairi DA, Alsabah BH, Alkhaledi BA, Pennekamp P, Omran H. Identification of a novel founder variant in DNAI2 cause primary ciliary dyskinesia in five consanguineous families derived from a single tribe descendant of Arabian Peninsula. *Front Genet*. 2022;13:1017280–1017294. https://doi.org/10.3389/fgene.2022.1017280.
20. Al-Mutairi DA, Alsabah BH, Pennekamp P, Omran H. Mapping the most common founder variant in RSPH9 that causes primary ciliary dyskinesia in multiple consanguineous families of Bedouin Arabs. *J Clin Med*. 2023;12(20):6505–6520. https://doi.org/10.3390/jcm12206505.
21. Carr IM, Morgan J, Watson C, et al. Simple and efficient identification of rare recessive pathologically important sequence variants from next generation exome sequence data. *Hum Mutat*. 2013;34(7):945–952. https://doi.org/10.1002/humu.22322.
22. Watson CM, Crinnion LA, Gurgel-Gianetti J, et al. Rapid detection of rare deleterious variants by next generation sequencing with optional microarray SNP genotype data. *Hum Mutat*. 2015;36(9):823–830. https://doi.org/10.1002/humu.22818.
23. Carr IM, Camm N, Taylor GR, et al. GeneScreen: a program for high-throughput mutation detection in DNA sequence electropherograms. *J Med Genet*. 2011;48(2):123–130. https://doi.org/10.1136/jmg.2010.082081.
24. Margolis RH, Morgan DE. Automated pure-tone audiometry: an analysis of capacity, need, and benefit. *Am J Audiol*. 2008;17(2):109–113. https://doi.org/10.1044/1059-0889(2008/07-0047).
25. Fralinger DJ, Kraft DB, Rogers KJ, Thacker MM, Kruse RW, Franzone JM. The fate of the bent rod in children with osteogenesis imperfecta. *J Pediatr Orthop*. 2023;43(6):e465–e470. https://doi.org/10.1097/BPO.0000000000002409.
26. Chan E, DeVile C, Ratnamma VS. Osteogenesis imperfecta. *BJA Educ*. 2023;23(5):182–188. https://doi.org/10.1016/j.bjae.2023.01.005.
27. Carr IM, Bhaskar S, O'Sullivan J, et al. Autozygosity mapping with exome sequence data. *Hum Mutat*. 2012;34(1):50–56. https://doi.org/10.1002/humu.22220.
28. Lander ES, Botstein D. Homozygosity mapping: a way to map human recessive traits with the DNA of inbred children. *Science*. 1987;236(4808):1567–1570. https://doi.org/10.1126/science.2884728.
29. Abecasis GR, Cherny SS, Cookson WO, Cardon LR. Merlin—rapid analysis of dense genetic maps using sparse gene flow trees. *Nat Genet*. 2002;30(1):97–101. https://doi.org/10.1038/ng786.
30. Carr IM, Markham SA, Pena SD. Estimating the degree of identity by descent in consanguineous couples. *Hum Mutat*. 2011;32(12):1350–1358. https://doi.org/10.1002/humu.21584.
31. Lui JC, Raimann A, Hojo H, et al. A neomorphic variant in SP7 alters sequence specificity and causes a high-turnover bone disorder. *Nat Commun*. 2022;13(1):700. https://doi.org/10.1038/s41467-022-28318-4.
32. Tung JY, Ho JL, Wong R, Fung SC. Dental phenotype in an adolescent with osteogenesis imperfecta type XII. *BMJ Case Rep*. 2022;15(4):246554–246558. https://doi.org/10.1136/bcr-2021-246554.
33. Hayat A, Hussain S, Bilal M, et al. Biallelic variants in four genes underlying recessive osteogenesis imperfecta. *Eur J Med Genet*. 2020;63(8):103954. https://doi.org/10.1016/j.ejmg.2020.103954.
34. Ludwig K, Ward LM, Khan N, et al. Dominant osteogenesis imperfecta with low bone turnover caused by a heterozygous SP7 variant. *Bone*. 2022;160:116400. https://doi.org/10.1016/j.bone.2022.116400.
35. Whyte MP, Campeau PM, McAlister WH, et al. Juvenile Paget's disease from heterozygous mutation of SP7 encoding Osterix (specificity protein 7, transcription factor SP7). *Bone*. 2020;137:115364. https://doi.org/10.1016/j.bone.2020.115364.
36. Dror AA, Avraham KB. Hearing impairment: a panoply of genes and functions. *Neuron*. 2010;68(2):293–308. https://doi.org/10.1016/j.neuron.2010.10.011.
37. Carre F, Achard S, Rouillon I, Parodi M, Loundon N. Hearing impairment and osteogenesis imperfecta: literature review. *Eur Ann Otorhinolaryngol Head Neck Dis*. 2019;136(5):379–383. https://doi.org/10.1016/j.anorl.2019.05.004.
38. Paterson CR, Monk EA, McAllion SJ. How common is hearing impairment in osteogenesis imperfecta? *J Laryngol Otol*. 2001;115(4):280–282.

39. Joseph JK, Maharaj SH. Osteogenesis imperfecta and hearing loss in the paediatric population. *Int J Pediatr Otorhinolaryngol*. 2021;150:110914. https://doi.org/10.1016/j.ijporl.2021.110914.
40. DeLaurier A, Eames BF, Blanco-Sanchez B, et al. Zebrafish sp7:EGFP: a transgenic for studying otic vesicle formation, skeletogenesis, and bone regeneration. *Genesis*. 2010;48(8):505–511. https://doi.org/10.1002/dvg.20639.
41. Renn J, Winkler C. Osterix/Sp7 regulates biomineralization of otoliths and bone in medaka (*Oryzias latipes*). *Matrix Biol*. 2014;34:193–204. https://doi.org/10.1016/j.matbio.2013.12.008.
42. Park JS, Baek WY, Kim YH, Kim JE. In vivo expression of Osterix in mature granule cells of adult mouse olfactory bulb. *Biochem Biophys Res Commun*. 2011;407(4):842–847. https://doi.org/10.1016/j.bbrc.2011.03.129.
43. Olmsted-Davis EA, Salisbury EA, Hoang D, et al. Progenitors in peripheral nerves launch heterotopic ossification. *Stem Cells Transl Med*. 2017;6(4):1109–1119. https://doi.org/10.1002/sctm.16-0347.
44. Swinnen FK, Coucke PJ, De Paepe AM, et al. Osteogenesis imperfecta: the audiological phenotype lacks correlation with the genotype. *Orphanet J Rare Dis*. 2011;6(1):88. https://doi.org/10.1186/1750-1172-6-88.
45. Pillion JP, Shapiro J. Audiological findings in osteogenesis imperfecta. *J Am Acad Audiol*. 2008;19(8):595–601.
46. Pillion JP, Vernick D, Shapiro J. Hearing loss in osteogenesis imperfecta: characteristics and treatment considerations. *Genet Res Int*. 2011;2011:983942–983948.
47. Hojo H, Ohba S. Sp7 action in the skeleton: its mode of action, functions, and relevance to skeletal diseases. *Int J Mol Sci*. 2022;23(10) 5647–5659. https://doi.org/10.3390/ijms23105647.
48. Hojo H, Ohba S, He X, Lai LP, McMahon AP. Sp7/Osterix is restricted to bone-forming vertebrates where it acts as a dlx co-factor in osteoblast specification. *Dev Cell*. 2016;37(3):238–253. https://doi.org/10.1016/j.devcel.2016.04.002.
49. Timpson NJ, Tobias JH, Richards JB, et al. Common variants in the region around Osterix are associated with bone mineral density and growth in childhood. *Hum Mol Genet*. 2009;18(8):1510–1517. https://doi.org/10.1093/hmg/ddp052.
50. Styrkarsdottir U, Halldorsson BV, Gretarsdottir S, et al. New sequence variants associated with bone mineral density. *Nat Genet*. 2009;41(1):15–17. https://doi.org/10.1038/ng.284.
51. Rivadeneira F, Styrkarsdottir U, Estrada K, et al. Genetic factors for osteoporosis, twenty bone-mineral-density loci identified by large-scale meta-analysis of genome-wide association studies. *Nat Genet*. 2009;41(11):1199–1206. https://doi.org/10.1038/ng.446.